



Optimizing Tall Masonry Walls with Partially Unbonded Guided Post-Tensioning

Mahmoud Elsayedⁱ, Rafael Gonzalezⁱⁱ, Alan Alonsoⁱⁱⁱ, Clayton Pettit^{iv}, Douglas Tomlinson^v, and Carlos Cruz-Noguez^{vi}

ABSTRACT

Tall masonry walls are widely used in single-story structures such as warehouses, schools, and industrial facilities. However, their high slenderness ratios (height/thickness) make them susceptible to second-order moments, often necessitating thicker walls and limiting their viability. While post-tensioning (PT) techniques have proven effective in reducing tensile stresses and member thickness in high-span reinforced concrete structures, their application in tall masonry walls remains relatively unexplored. In this study, the use of partially unbonded guided PT techniques to enhance the performance of tall masonry walls is investigated. A full-scale concrete masonry wall with a height of 8.75 metres and a slenderness ratio of 46 was experimentally tested under realistic loading and different boundary conditions. The wall was subjected to eccentric vertical loads and uniform out-of-plane pressures using an airbag, simulating conditions typical of one-story structures. The test objective was to investigate the effect of the applied PT stress, the presence of eccentric vertical load, and the effect of the base condition on the out-of-plane response of the PT masonry wall. The results indicate that using a fixed base and/or increasing the applied PT stress improves the response of the wall up to the serviceability limits. Additionally, the findings reveal that even with low levels of applied PT force, PT masonry walls can outperform or exhibit behaviour comparable to walls reinforced with conventional mild steel.

KEYWORDS

Tall masonry walls, unbonded post-tensioning bars, Out-of-plane response, Full-scale experimental testing

ⁱ PhD Candidate, University of Alberta, Edmonton, Canada, mhelsaye@ualberta.ca

ⁱⁱ PhD Candidate, University of Alberta, Edmonton, Canada, rgonzalez@ualberta.ca

ⁱⁱⁱ Structural Engineer, RJC Engineers, Edmonton, Canada, aalonsorivers@rjc.ca

^{iv} Assistant Professor, University of Alberta; Edmonton, Canada, cpettit@ualberta.ca

^v Associate Professor, University of Alberta, Edmonton, Canada, dtomlins@ualberta.ca

^{vi} Professor, University of Alberta, Edmonton, Canada, carlos.cruznoguez@ualberta.ca



INTRODUCTION

The post-tensioning (PT) technique originated in the early 20th century when engineers sought methods to enhance the strength and efficiency of reinforced concrete (RC) structures. Although prestressing concepts were first proposed by engineers like Eugène Freyssinet in 1928 [1], PT systems gained practical application only after the development of high-strength steel in the 1930s [2]. This innovation was driven by the need to overcome the limitations of plain and reinforced concrete, such as cracking under small tensile stresses and excessive deflections in long-span members. Following this, the adoption of PT techniques expanded globally, with notable applications in bridge construction and large-span structures emerging in the late 1950s across Europe and the United States [3].

Currently, PT reinforcement is widely used in RC structures for various applications, including tilt-up walls. PT reinforcement reduces wall thickness and, consequently, weight, facilitating transportation and lifting processes while maintaining adequate load-carrying capacity. However, despite its extensive adoption in RC structures, post-tensioning has seen limited application in masonry construction, even though masonry walls face similar design challenges and could benefit from PT reinforcement advantages.

PT reinforcement in masonry is not entirely new, and numerous studies have demonstrated potential benefits [4]. Research on masonry flexural members, such as beams and walls, consistently shows that post-tensioning enhances both cracking and ultimate flexural strengths [5-8]. Key findings include that restrained (guided) or bonded PT bars outperform unrestrained (unguided) ones, as the latter significantly reduce post-cracking capacity and stiffness and may lead to compression-controlled failure. Restrained PT bars with high PT forces can prevent hinge formation, a common failure mode in unbonded PT slender walls [9], highlighting the importance of lateral restrainers when using PT reinforcement. The PT bars can be restrained laterally using mechanical restrainers or filling certain blocks with grout or mortar [10]. Due to their higher capacity and favourable failure mode, grouted restrainers over others, such as mortar or steel, are recommended.

Other studies [9, 11, 12] have examined the effects of the slenderness ratio on the behaviour of unbonded PT masonry walls. These studies reported that increasing the slenderness ratio reduces flexural resistance due to the magnification of secondary moments ($P\delta$). Popohn and Schultz [13] used finite element analysis to study PT masonry walls under various conditions and imperfections. Their findings emphasize that masonry tensile strength is critical for determining peak load capacity, and imperfections can significantly affect flexural strength, particularly in walls with high slenderness ratios.

Although significant progress has been made in understanding PT masonry systems, existing research has primarily focused on walls with limited slenderness ratios and heights below 6000 mm. The combined use of mild steel and post-tensioning reinforcement in partially post-tensioned systems remains underexplored. To the authors' knowledge, only Garwood [5] conducted tests on partially post-tensioned masonry beams, leaving a gap in the literature on tall masonry walls. This study seeks to fill this gap by investigating the behaviour of tall masonry walls with a slenderness ratio of 46, incorporating both mild and post-tensioning reinforcement to evaluate their structural performance and potential for practical implementation.

RESEARCH PROGRAM

This study is part of a comprehensive research program at the University of Alberta aimed at enhancing the performance and constructability of tall masonry walls. The program has explored various aspects of wall behaviour and design, including the impact of base stiffness on structural performance [14], the development of a stiffness coefficient (k) to account for base rigidity [15], and the improvement of flexural stiffness by placing reinforcement to the edge of the hollow cells in the blocks [16]. Additionally, the

research addressed constructability challenges by introducing an offsite construction solution for tall masonry walls [17]. Building on these efforts, the current study investigates the application of unbonded post-tensioning (PT) tendons as an approach to improving the performance of tall masonry walls.

Test Specimen

Figure 1 shows the specimen details. The post-tensioned wall (PTW) measured 8750 mm in height and 1190 mm in width, constructed using standard concrete masonry units of 20 cm (19 cm thick), resulting in a slenderness ratio of 46. The reinforcement configuration was designed to demonstrate that tall masonry walls reinforced with unbonded PT reinforcement can perform comparable or superior to conventionally reinforced walls. The reinforcement layout was selected to match the nominal moment capacity (M_n) of 18 kNm observed in conventional walls (CW) tested by Alonso et al. [14], calculated using the equations provided in CSA S304-24 [18] and TMS 402-22 [19].

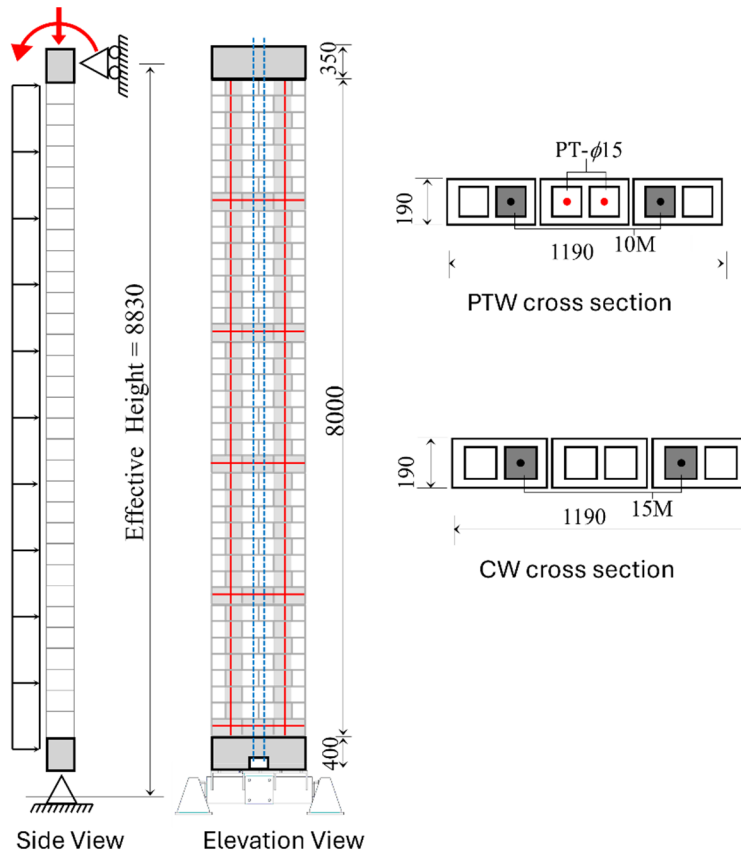


Figure 1. Details of the test specimens (units in mm).

The M_n for masonry walls reinforced with a combination of unbonded PT tendons and mild steel bars can be determined using Eq. (1). The stress in the unbonded PT bars at nominal capacity, denoted as f_p , can be calculated using Eq. (2) from CSA S304-24 or Eq. (3) from TMS 402-22. Key parameters include l_p , the distance between the anchorage ends of the PT bars; d_p , the distance from the extreme compression fibre to the PT bar; c , the depth of the compression block; E_p , the Young's modulus of the PT bars; P , the applied vertical load; A_p , the area of the PT bars; and b , the width of the cross-section.

$$(1) M_n = A_s f_y (d - \beta c) + A_p f_p (d - \beta c) + P \left(\frac{t}{2} - \beta c \right)$$

$$(2) f_p = f_{pe} + \frac{E_p}{25 l_p} (d_p - c)$$

$$(3) f_p = f_{pe} + \frac{0.03 \left(\frac{E_p d_p}{l_p} \right) \left(1 - 1.56 \frac{A_p f_{pe} + P}{f_m b d} \right)}{1 + 0.0468 \left(\frac{E_p A_p}{f_m b l_b} \right)}$$

While unbonded PT reinforcement alone can achieve the required M_n , it is not recommended for exterior walls due to wide crack openings during out-of-plane (OOP) deformation and increased susceptibility to corrosion [8]. Bonded reinforcement mitigates these issues by ensuring strain compatibility and transferring tensile stresses from the grout to the reinforcement, which helps limit crack widths. Therefore, this study uses a combination of mild steel reinforcement and PT bars. Two 10M bars ($2 \times 100 \text{ mm}^2$) spaced at 600 mm, combined with two $\text{Ø}15$ unbonded PT bars ($2 \times 177 \text{ mm}^2$), are used to achieve the required M_n , depending on the applied PT forces. Figure 2 illustrates the expected nominal capacities for the PTW, based on the proposed reinforcement configuration and the material properties discussed later, under varying levels of f_p . The results indicate that both CSA S304-24 and TMS 402-22 have similar M_n values, with CSA providing slightly higher estimates. The targeted M_n is achieved when f_p is approximately 20% of the PT bars yield strength (f_{py}). The CSA S304-24 restricts the use of unrestrained (unguided) PT bars in masonry walls based on the findings of the literature; therefore, bond beams were used every eight courses to serve as lateral restrainers.

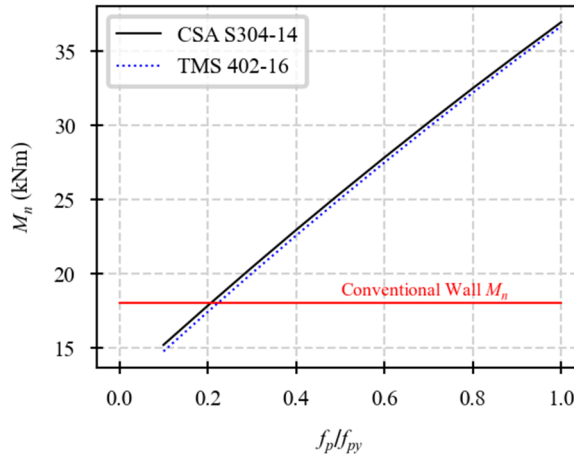


Figure 2. Expected nominal capacity for the PTW

Experimental setup

The experimental setup consists of a steel truss with fixtures at the top as vertical roller support and a base that can vary from free-rotating to fixed by adding stiff steel pedestals, as shown Fig. 3. This configuration was described earlier [20]. An eccentric vertical load was applied to the top of the wall by suspending weights from a lever arm. The load was transferred to a plate attached to the upper part of the wall. Load cells were placed between each lever arm, and the plate affixed to the wall to measure the applied vertical load. Load cells were also used to monitor the PT force during the jacking and test. Out-of-plane loads were applied by inflating an airbag between the frame and the wall. A series of cable transducers connected to the steel structure measured the out-of-plane displacements. A pressure gauge attached to the airbag measured the pressure within it.

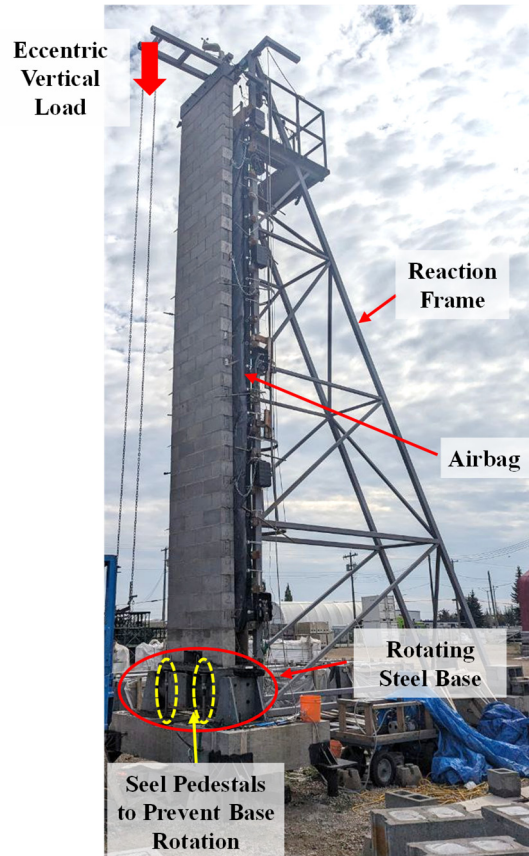


Figure 3. Experimental testing setup

Materials

Pre-mixed Type S mortar and coarse grout with specified compressive strengths of 12.5 MPa and 20.6 MPa, respectively, were used. Six mortar cubes measuring $50 \times 50 \times 50$ mm were tested under concentric axial loads per CSA A179 [21], resulting in an average compressive strength of 21.7 MPa (COV = 6.5%). Four cylindrical grout specimens (100×200 mm) were similarly tested according to CSA A179, resulting in an average compressive strength of 26.4 MPa (COV = 7.7%).

Grade 400 steel reinforcement was utilized for the bonded reinforcement, and three 10M steel bar coupons were tested following ASTM A615 [22]. These bars exhibited an average yield strength of 474 MPa (COV = 2.4%) and an elastic modulus of 189 GPa (COV = 1.94%). The PT bars used in the study had a diameter of 15 mm (176 mm^2) and were made of Grade 900/1100 MPa steel. Testing of the PT bars coupons showed an average yield strength of 1043 MPa (COV = 0.85%) and an elastic modulus of 209 GPa (COV = 0.85%). The compressive strengths of masonry prisms were evaluated by testing five grouted and five ungrouted prisms following CSA S304-24, which resulted in average strengths of 28.6 MPa and 17.6 MPa, respectively.

Loading Protocols

Although a PT stress of 20% f_{py} is sufficient to achieve a similar M_n as the CW, the PT stress was varied during testing to examine how changes in the PT force influence the service performance of the PTW. Other factors, including an axial load of 15 kN with a 170 mm eccentricity and the base conditions, were adjusted to examine their effects on wall behaviour. The loading protocol used is shown in Fig. 4.

The testing protocol consists of ten phases designed to evaluate wall performance under different stages, such as uncracked, cracking, serviceability, yielding, and failure states. The phase identifiers in Fig. 4 begin with the letter "P" (indicating the phase), followed by the phase number and "F" or "H" to denote fixed or hinged base conditions. The subsequent percentage indicates the PT force as a fraction of f_{py} , and the final letters "EL" or "NEL" specify whether eccentric vertical loading is applied. For instance, "P2-H-20%-NEL" represents the second phase, during which the wall was tested with a hinged base condition, a PT force of 20% f_{py} , and without eccentric vertical load. This axial load was selected to replicate the loading conditions of the CW [14].

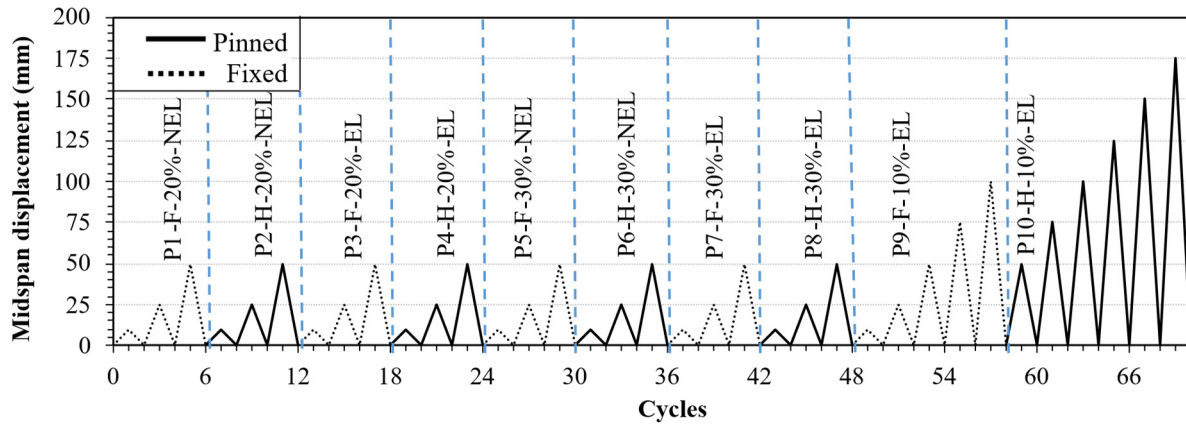


Figure 4. Load protocol for the PTW

RESULTS AND DISCUSSION

Load-displacement response

The load-displacement histories for the PTW during the service cycles are presented in Fig. 5. The load-displacement response exhibited bilinear behaviour throughout all cycles up to the serviceability displacement limit (50 mm) regardless of the applied PT force, base condition, or the presence of eccentric vertical loading. The initial segment of the bilinear curve corresponds to the elastic, uncracked state of the wall, while the second segment represents the elastic, cracked state. Although the wall exhibited cracking from the first cycle, the bilinear response persisted for all subsequent phases due to the restoring force provided by the unbonded PT reinforcement.

At the end of each cycle, the residual midspan displacement was minimal, allowing the cracks to close and the wall to return to its uncracked state. This behaviour is further reflected in the narrow hysteresis loops, which indicate limited energy dissipation. The narrow loops suggest that the wall did not dissipate significant energy through cracking or reinforcement yielding, as the unbonded PT bars maintained their linear elastic behaviour throughout.

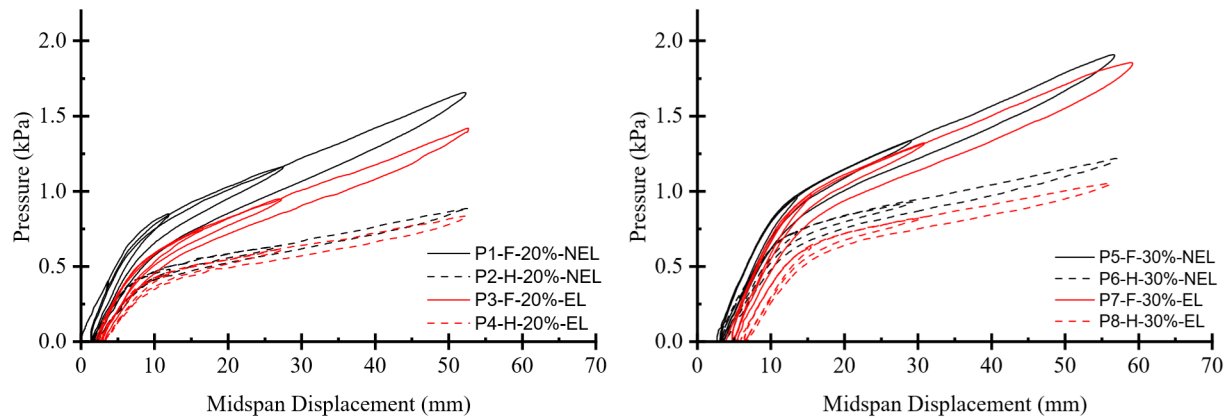


Figure 5. Load displacement history for service cycles of the PTW

The base condition was observed to be the most significant factor influencing the performance of the wall. Using a fixed base condition resulted in a noticeably higher post-cracking slope (stiffness), which enhanced the wall resistance to the applied OOP pressure. At the service displacement of 50 mm, the pressure resistance of the PTW with a fixed base was at least 1.6 times greater than that of the same wall with a hinged base. This highlights the importance of considering a fixed base condition, as it effectively reduces midspan displacement under a given applied pressure by redistributing the moments along the wall height, thereby minimizing second-order moments [15].

The PT force was the second most influential parameter observed in the behaviour. Increasing the PT force enhanced both the cracking and service pressure resistances of the wall. The improvement in the cracking pressure resistance is attributed to the higher compressive forces, which require a greater applied moment to counteract these forces and initiate cracking in the wall. Similarly, the increase in service pressure resistance is due to the effect of higher concentric compression forces on the section, which improves the sectional stiffness and, consequently, the resistance of the wall to applied pressure [23].

The final parameter considered was the presence of an eccentric axial load. Applying a 15 kN load at 170 mm eccentricity was found to have no significant impact on the performance of the PTW. Although the moment induced by load eccentricity and second-order effects could potentially reduce the pressure resistance of the wall, the additional compression force appeared to enhance the section resistance, as previously discussed. Under service conditions, the midspan displacement was not substantial enough to generate large secondary moments, further minimizing the impact of the eccentric axial load.

It is important to note that during the P1 phase, the wall exhibited the cracking resistance of the masonry assembly, resulting in a noticeable difference from the P3 phase. However, this difference was attributed to the inherent cracking resistance of the masonry assembly rather than the influence of the eccentric axial load.

The load-displacement histories for the PTW during the yielding cycles are shown in Fig. 6. In these cycles, the PTW demonstrated a trilinear load-displacement response. The first two segments correspond to the uncracked and cracked stages, similar to the behaviour observed during the service cycles in Fig. 5. The third segment represents the yielding stage, during which the mild steel bars reached their yield point.

In P9, strain gauges attached to the mild bars at the first course recorded readings close to the yield strain at approximately 80 mm of midspan displacement. This was accompanied by a noticeable reduction in the slope of the load-displacement curve. The P9 phase concluded at 130 mm of midspan displacement with a

pressure resistance of 1.94 kPa to prevent failure before proceeding to the P10 phase. Upon unloading in the final cycle of P9, the hysteresis loop was observed to be wide, confirming the yielding of the mild bars and the associated energy dissipation through the yielding process.

In P10, the yielding of the mild bars was immediately evident, as indicated by a significant residual displacement of 10 mm carried over from P9, compared to the minimal residual displacements in earlier cycles. Despite this, the P10 phase displayed a similar load-displacement response, with distinct uncracked and cracked stages. At approximately 112 mm midspan displacement, an unexpected increase in the slope of the load-displacement curve was observed. This may be attributed to unforeseen grout leakage during construction, which likely introduced additional restraint within the cells containing the unbonded PT bars.

Increasing the number of lateral restraints has been shown to enhance wall stiffness, as noted by Popehn [12]. It is assumed that the unbonded PT bars experienced additional restraint at this displacement, contributing to the observed increase in pressure resistance. The P10 phase concluded at a midspan displacement of 185 mm, with a pressure resistance of 1.43 kPa, after a sudden drop in the load-displacement response was observed.

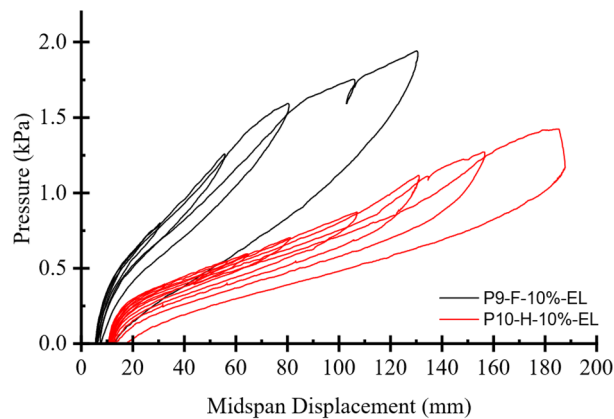


Figure 6. Load displacement history for yielding cycles of the PTW

Comparison with conventionally reinforced walls

The load-displacement envelopes for the PTW (from this study) and CWs (tested by [14]) are presented in Fig. 7. The CWs were two identical specimens with the same overall dimension and loading condition of the PTW. One of the CWs was tested with a hinged base, and the other was tested with a fixed base. To ensure comparable loading conditions, the figures include only the envelopes for cycles with a 15 kN eccentric load. The reinforcement configuration of the CWs is shown in Fig. 1. While the reinforcement configurations of the CWs and PTW differ significantly, this comparison aims to demonstrate the feasibility of the proposed reinforcement configuration used in this study.

As outlined in the test specimen section, the reinforcement configuration for the PTW was designed to achieve the same M_n as the CW. Initial calculations suggested that f_p equal to $20\% f_{py}$ would produce the same M_n . However, testing revealed that this PT stress level provided greater pressure (and moment) resistance than the CWs. Consequently, the PT stress was reduced to $10\% f_{py}$. At this reduced stress level, the PTW achieved moment resistance comparable to that of the CWs, as shown in Fig. 7b for the fixed base condition. For the hinged base condition, the PTW exhibited a similar load-displacement response to the CW up to the point of a sudden change in the slope of the PTW load-displacement curve, as shown in Fig. 7a. This highlights that both CSA S304 and TMS 402 underestimated the M_n for slender masonry walls reinforced with a combination of mild steel and unbonded PT bars.

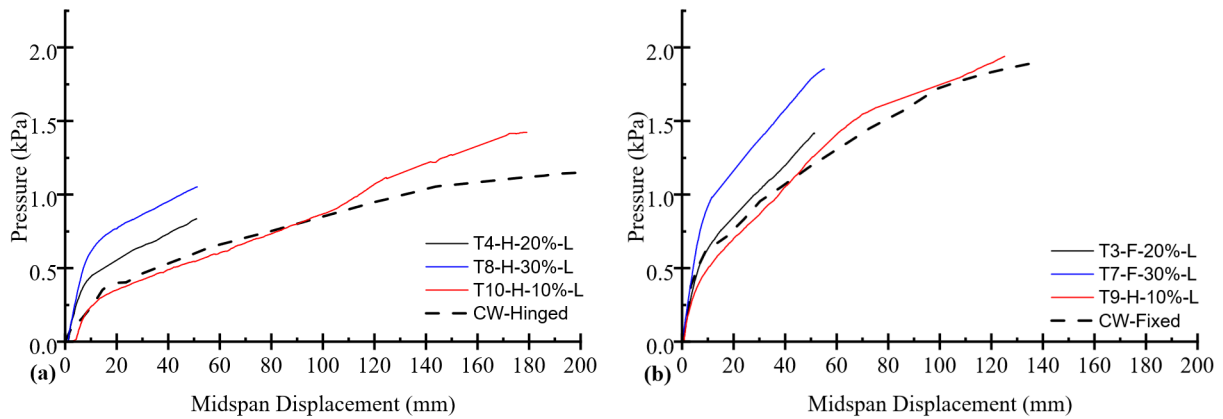


Figure 7. Load-displacement response envelopes for: a) hinged base & b) fixed case

CONCLUSION

This study investigated the performance of tall masonry walls reinforced with mild steel bars and unbonded post-tensioning (PT) bars. A full-scale specimen with a slenderness ratio of 46 was tested under combined eccentric axial load and cyclic out-of-plane pressure. Testing included ten cyclic phases with variations in PT forces (10%, 20%, and 30% of PT bar yield strength), base fixities (hinged and fixed), and eccentric vertical load. The key findings are:

- The unbonded PT reinforcement provided restoring forces, limiting residual displacements after unloading and ensuring the wall returned to an uncracked state during service cycles.
- The use of fixed base conditions significantly increased the post-cracking stiffness, resulting in pressure resistances at least 1.6 times greater than those of the hinged base condition at the service displacement of 50 mm.
- Larger PT forces enhanced both cracking and service resistance.
- Despite the presence of an eccentric axial load, the applied load values in this study did not result in any significant reduction in the pressure resistance of the wall.
- The load-displacement response for the yielding phases exhibited a trilinear behaviour, with the final segment attributed to the yielding of the mild steel bars.
- The PT wall (PTW) matched or exceeded the moment resistance of conventionally reinforced walls (CW) designed for the same nominal capacity, requiring only 10% of the PT bar yield strength (f_{py}) to achieve the same nominal moment capacity as the CW.

These results confirm that combining mild reinforcement with unbonded PT tendons is a viable approach for tall masonry walls, offering enhanced performance and the flexibility to adjust PT levels to accommodate service and post-cracking behaviour. Future studies should investigate the long-term effects of cyclic loading on PT systems, larger PT levels, larger applied eccentric loads and potential shifts in failure modes.

ACKNOWLEDGEMENTS

The authors wish to acknowledge the generous contributions and donations from the Masonry Contractors Association of Alberta (MCAA), the Alberta Masonry Council (AMC), Canadian Concrete Masonry Producers Association (CCMPA), the Discovery Grant program (NSERC), the Canadian Masonry Design Centre (CMDC), SCORPIO Masonry, EXPOCRETE, and Dywidag.

REFERENCES

- [1] K. W. Shushkewich, "Eugène Freyssinet—Invention of Prestressed Concrete and Precast Segmental Construction," *Struct. Eng. Int.*, vol. 22, no. 3, pp. 415–420, 2012, doi: 10.2749/101686612x13363869853338.
- [2] M. Wyrzykowski, G. Terrasi, and P. Lura, "Chemical prestressing of high-performance concrete reinforced with CFRP tendons," *Compos. Struct.*, vol. 239, p. 112031, 2020, doi: 10.1016/j.compstruct.2020.112031.
- [3] S. Kamalakannan, R. Thirunavukkarasu, R. G. Pillai, and M. Santhanam, "Factors affecting the performance characteristics of cementitious grouts for post-tensioning applications," *Constr. Build. Mater.*, vol. 180, pp. 681–691, 2018, doi: 10.1016/j.conbuildmat.2018.05.236.
- [4] S. L. Lisse, E. Y. Sayed-Ahmed, and N. G. Shrive, "Prestressed Masonry—The Last Ten Years," presented at the 8th North American Masonry Conference (8NAMC), 1999.
- [5] T. G. Garwood, "A Comparison of the Behaviour of Reinforced, Prestressed and Partially Prestressed Brickwork Beams," *Proc. Br. Masonry Soc.*, no. 2, pp. 76–81, 1988.
- [6] K. J. Graham and A. W. Page, "An Experimental Study of the Flexural Behaviour of Post-Tensioned Hollow Clay Masonry," *Calgary*, Jul. 1994, pp. 639–648.
- [7] R. Rodriguez, A. A. Hamid, and J. Larralde, "Flexural Behavior of Post-Tensioned Concrete Masonry Walls Subjected to Out-of-Plane Loads," *ACI Struct. J.*, vol. 95, no. 1, 1998, doi: 10.14359/527.
- [8] H. P. Miranda, L. R. Feldman, and B. F. Sparling, "Proof of concept investigation of unbonded reinforcement in concrete block masonry," *Can. J. Civ. Eng.*, vol. 45, pp. 936–946, 2018, doi: 10.1139/cjce-2017-0578.
- [9] J. R. B. Popehn, A. E. Schultz, and C. R. Drake, "Behavior of Slender, Posttensioned Masonry Walls under Transverse Loading," *J. Struct. Eng.*, vol. 133, no. 11, pp. 1541–1550, Nov. 2007, doi: 10.1061/(asce)0733-9445(2007)133:11(1541).
- [10] D. D. Stierwalt and H. R. Hamilton, "Restraint Effectiveness in Unbonded Tendons for Prestressed Masonry," *ACI Struct. J.*, vol. 97, no. 6, 2000, doi: 10.14359/9629.
- [11] E. M. Lacika and R. G. Drydsale, "Experimental Investigation of Slender Prestressed Brick Walls," presented at the 7th Canadian Masonry Symposium, Jun. 1995.
- [12] J. R. B. Popehn, A. M. Asce, and A. E. Schultz, "Finite-Element Models for Slender, Posttensioned Masonry Walls Loaded Out-of-Plane," *J. Struct. Eng.*, vol. 137, pp. 1489–1498, Mar. 2011, doi: 10.1061/(asce)st.1943-541x.0000411.
- [13] J. R. B. Popehn and A. E. Schultz, "Influence of imperfections on the out-of-plane flexural strength of post-tensioned masonry walls," *Constr. Build. Mater.*, vol. 41, pp. 942–949, Apr. 2013, doi: 10.1016/j.conbuildmat.2012.07.016.
- [14] Alonso et al., "Experimental Testing of Tall Slender Masonry Walls with Different Rotational Base Stiffnesses," *J. Struct. Eng.*, vol. 150, no. 3, p. 04024010, 2024, doi: 10.1061/jsendh.steng-12533.
- [15] Alonso, "Influence of Foundation Rigidity on the Out-of-Plane Flexural Response of Slender Masonry Walls," Ph.D. dissertation, University of Alberta, 2023.
- [16] R. Gonzalez, A. Alonso, M. Elsayed, C. Cruz-Noguez, and D. Tomlinson, "Response of a Partially-Grouted Slender Masonry Wall with an Alternative Steel Reinforcement Arrangement," in *Proc. 18th Int. Brick Block Masonry Conf.*, 2025, pp. 184–194, doi: 10.1007/978-3-031-73310-9_13.
- [17] M. Elsayed, A. Alonso-Rivers, R. Gonzalez, S. Adeeb, D. Tomlinson, and C. Cruz-Noguez, "Constructability of Segmental Concrete Masonry Tall Walls," in *Masonry 2022: Advancing Masonry Technology*, pp. 87–102, Dec. 2022, doi: 10.1520/stp164020210117.
- [18] CSA S304-24, *Design of Masonry Structures*. CSA Group, 2024.
- [19] TMS 402/602-22, *Building Code Requirements and Specification for Masonry Structures*. The Masonry Society, 2022.

- [20] CSA A179-14, Mortar and Grout for Unit Masonry. CSA Group, 2014.
- [21] ASTM A615, Standard Specification for Deformed and Plain Carbon-Steel Bars for Concrete Reinforcement. ASTM, 2022.
- [22] Sparling and D. Palermo, "Response of Full-Scale Slender Masonry Walls with Conventional and NSM Steel Reinforcement Subjected to Axial and Out-of-Plane Loads," *J. Struct. Eng.*, vol. 149, no. 1, p. 04022208, 2023, doi: 10.1061/jsendh.steng-11364.